Multi-bands image analysis using local fractal dimension.

AURA CONCI[1]
ÉLDMAN DE OLIVEIRA NUNES[1]
[1]Instituto de Computação – UFF, R Passo da Pátria 156, 24210-240, Niterói, RJ, Brasil
aconci@ic.uff.br, eldman@bol.com.br

Abstract. An important application of fractals is image texture analysis. The main aspect of fractal geometry used in this application is the concept of fractal dimensions to characterize the texture-scaling behavior. A new idea is presented here: the use of fractals for texture identification in multiband image analysis. This is not a simple extension of the usual characterization of multifractal from its local dimension in gray-level images. It is related to examine the interrelationship among the image representation in bands. Moreover, each band can be seen as a set in the 3D space, which means that its fractal dimension may present results between 2 and 3. Consequently, if two bands are considered in one gathering, their structure is a set in the 4D space and its fractal dimension may present results between 2 and 4. For multi-bands image the fractal dimension upper bound can be even larger. In this work, two propositions to handle the multi-band combination are presented. Both defined for whatever combination of bands. As far as we know, no similar approach has been considered until now.

1 Introduction

Multiband imaging often found in color application has been leading the research growth of a new global Earth information and satellite industry. The recent generation of imagery acquisition products, in addition to the spatial resolution (which allows to distinguish objects on the Earth's surface as small as one meter in size), has been increased also in the range and number of multispectral bands. Visible light is composed of wavelengths ranging from 0.4μm (Blue) to 0.7μm (Red). This narrow portion of the electromagnetic spectrum is the entire range to which the human eye is sensitive. Landsat Thematic Mapper-TM sensors collect data from Blue to Red (Band 1:0.54-0.52 μm, Band 2-0.52-0.60μm and Band 3-0.63-0.69μm) and beyond the Red end of the visible wavelength, where there are three regions of infrared energy waves: the near-infrared (Band 4-0.76μm to 0.90μm), the mid-infrared (Band 5-1.55μm to 1.75μm and Band 7-2.08μm to 2.35μm) and the thermal infrared (Band 6-10.4μm to 12.5μm).

From military purposes to commercial Geographic Information Systems (GIS), the use of this multiband image processing has also grown fast. For many tasks related to such applications, images need to be segmented so that, for example, areas at different times and economical utilization can be compared. Each band has special uses in this endeavor. Usually hot objects (forest fires, lava flows and emissions from smokestacks) have peaks that falls between 0.5μm to 9.5μm and thus can be detected in Bands 5 and 7. Band 6 is designed to measure surface temperatures (from -100^{o}C to 150^{o}C). In addition, the high transmittance of mid-infrared wavelengths means that Bands 5 and 7 penetrate smoke that obscures pinpointing fires in Bands 1 to 3.

The fraction of energy reflected at a particular wavelength varies with different earth features. Moreover, the reflectance of each earth feature varies at different wavelength. Thus two features that are indistinguishable in one spectral range may be very different in another wavelength band and the image spectral information can be used to distinguish regions. For example, in case of Earth observation the main distinguishable aspects are related to soil, building constructions, vegetation, water, smokes, clouds and trafficability. Soil texture, surface roughness and the presence of moisture (Iron oxide, organic matter, etc) can reduce soil reflectance in visible region (Bands 1-3), but the decrease of soil reflectance from moisture influence are most notable in Bands 5 and 7, which provide useful information for building constructions and soil trafficability. Vegetation reflectance varies during its cycle of growth. Pigments in plant leaves dictate the reflectance in visible bands. Chlorophyll strongly absorbs energy in wavelengths of 0.45μm and 0.67μm. Healthy vegetation appears green because of the relatively high reflection of green energy by plant leaves and the high absorption of blue and red. In near infrared (Band 4), reflectance is determined by the cellular structure, and in the mid-infrared (Band 5 and 7), reflectance is due to plant water content. A water region tends to be darker than its surrounding vegetation region. The visible bands provide information on water turbidity, bathymetry, currents and sediment plumes. In Bands 1 to 3 the energy reaching the sensor from the water may be reflected from the surface, from particles in the water or from the bottom if the water is clear and shallow. Water

body containing large quantities of suspended sediment normally has higher reflectance than clear water in the same area. Because water absorbs energy at infrared wavelengths, the infrared bands are used to easily locate and delineate water bodies.

TM Bands 1 to 5 and 7 measure reflected energy. TM Band 6, the thermal band, measures emitted energy. The data acquired from each of these bands can be viewed individually as a single band gray-level image. In single band images, energy intensity is represented in varying tones of gray. Color imagery is usually produced by combining single-band images is a computer, assigning one color per band (Red,Green or Blue) and then producing a colored output. As well as each band has special application; their combinations in color images allow different analysis. For instance, the combination of Band 4 (as Red), Band 5 (as Green) and Band 3 (as Blue) added definition of land-water boundaries and highlights subtle details not apparent in the visible bands alone. With this band combination, vegetation show as variations in hue as well as in tone, thus it is useful for analysis of soil and vegetation conditions. By displaying Band 4 as Red, Band 3 as Green and Band 2 as Blue, the human eye easily discriminates subtle tone variation chlorophyll reflectance and information can be gleaned about conditions and variety of vegetation.

Although TM sensor bands have been here considered to illustrate, similar approaches of multi-bands combinations can be used with others multi-bands sensor. A similar situation appears with the space imaging sensors Haute Resolution Visible-HRV and Advanced Very High Resolution Radiometer (AVHRR) of SPOT and NOAA satellite, respectively. Also in other applications, combinations of different multi sensor data of the same image (like the visible RGB and x-ray used for quality control) can be used to improve the analysis.

However, combining band's information is not the ultimate solution that can be gleaned. There are still problems of distinguishing region with same characteristic of reflectance unless textural information is used. Texture classifications allow to identify regions having a similar gray or color value into different objects if their present patterns variations. Different woods and residential regions are characterized by their high-contrast texture. Fields, lakes and seas present smooth contrast in tone and hue but highly different texture. Kinds of agricultural fields have different texture regions that can be useful on located their boundaries. So the next step in improving image analysis is joining the multi-bands possibilities with texture analysis.

In this paper, we propose a new idea by combining texture analysis in a multiband study of fractal dimension. It is not only related to the use of fractals to identify variation on texture in an image, but with the use of any images combination of the same scene to identify the texture. Nevertheless, for real world images some properties and problems are related with fractal dimension estimation, as discussed below (next section). Approaches for combining the bands for texture analysis are then proposed in section 3. They are very efficient computationally, and suitable for texture image recognition. We illustrate their use to image bands in section 4. Finally, in section 5, we present the conclusions of the proposed methodology.

2 Fractal dimension in gray-level images

Fractal geometry can be use to discriminate between textures in self-similar sets. The word fractal refers to entities (in present study sets of pixels) that display a degree of self-similarity at different scales. Altought Hausdorff dimension is the principal definition of dimension in this geometry; for real images it is a problem to implement algorithm for efficient Hausdorff dimension estimation (Conci and Monteiro, 2000). However, other definitions are in widespread use, and it is appropriate examine some of these alternative definitions of dimension (that can be used as an attempt to quantify and classify textures of a set of pixels). The fractal dimensions of a set A in Euclidean n-space can be derived from $1= N_r r^{FD}$:

$$FD = \log (N_r) / \log(1/r) \qquad (1)$$

where N_r is the union of non-overlapping copies of A scaled down by a ratio r.

For calculating fractal dimensions (FD) of drawable sets, the box-counting or box dimension (where B&W sketch is considered 2-D) is the most widely used dimension. Its calculation is relatively ease. This FD has been called also entropy dimension, Kolmogorov entropy, capacity dimension, metric dimension, logarithmic density, information dimension and Minkowski dimension (Falconer, 1997). This dimension provides a description of how much of the surface a set fills. White pixels are related with mass spread (area filled by the draw) and the Black pixels characterize gaps (or vice-versa), that is the area without mass distribution. If a set $A \varepsilon \Re^2$ is covered by just-touching boxes of side with length $\varepsilon=(1/2)^n$ (figure 1), equation (1) can be rewriting for experimental propose as

$$FD = \lim_{n \to \infty} (\log N(A , \varepsilon)) / (\log 1/\varepsilon) \qquad (2)$$

where $N_{(A , \varepsilon)}$ denotes the number of boxes of side length $\varepsilon=(1/2)^n$ which intersect the set A.

In algorithms, the image division in box of different length is processed in a simple way: considering that the image of M x M pixels has been partitioned into grids of sxs pixels and scaled down to r=s/M, then taking

contributions from all grids each $N_{(A, \varepsilon)}$ is computed. Then the limit in (2) can be estimate from the least-squares linear fit of log x log (figure 1).

However, an image fills all the underlined area. It is not possible associate a color with gaps, all spatial resolution pertains to the object. Gray-scale pictures or each band of multibanded images must be seen as an element of the space of functions

$$f : X \rightarrow G$$

where the set X is taken as the set of spatial coordinates of the image and G represents the set of intensity values of the image in a given band. So a simple extension of box-counting to gray scale images is by the assumption that it can be viewed as three-dimensional object (the third coordinate represent the pixel intensity as shown in figure 2), or as a terrain surface whose height is proportional to the image intensity value. The FD of an image can be derived from the relation (2), and one can expect results in all possible range of 3D surfaces for each band, that is from 2 to 3.

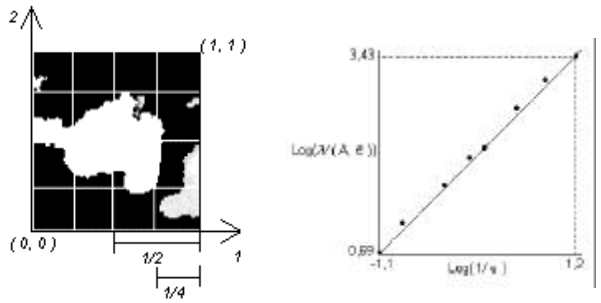

Figure 1 Elements for computation box-counting dimension: (left) the just-touching boxes covering the set A with side length $\varepsilon=1/2$ and $\varepsilon=(1/2)^2$. Boxes intersection with A and (right) least squares linear fit for estimation of the limit.

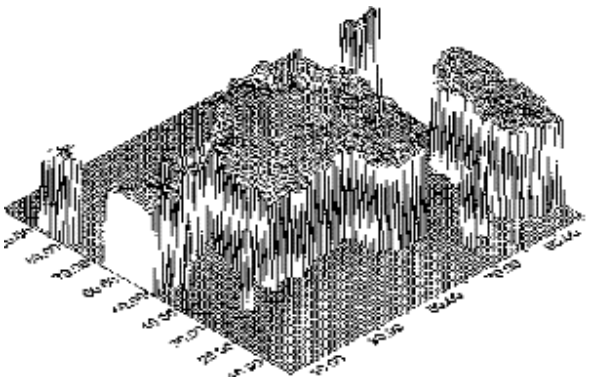

Figure 2 Gray intensity as third coordinate

Suppose the image of MxM pixels has been partitioned into grids of sxs pixels and scaled down to r=s/M. If G is the total number of gray levels then G/s'=M/s. On each grid there is a column of boxes of size sxsxs'. Assign number 1, 2, ...n to the boxes as shown in figure 3, the box counting $N_{(A , \varepsilon)}$ for FD computation in each band is a simple extension. Boxes are now 3D elements and $N_{(A , \varepsilon)}$ in equation (2) denotes the number of boxes of side length $\varepsilon=(1/2)^n$ which intersect the set A , also in the pixel intensity direction.

For images, the Blanket Method (Peleg et al. 1984), the Reticular Cell Counting (Gangepain and Roques-Carmes, 1986) or the DBC - Differential-Box Counting (Sarkar and Chaudhuri, 1994) are more adequate than equation (2) to compute the FD. All these are based on the Blanket Dimension or Blanket Covering Method, which is an extension of the Mandelbrot's method of measuring the length of a coastline. For a line curve it proposes drawing a strip around the coastline such that no part of the strip is more than a distance ε from the curve. Then the width of the strip is 2ε and the length of the coastline at radius ε is its area divided by 2ε. For a surface, Peleg et al.(1984) suggested that it have to be filled with a "blanket" such that all points on the blanket surface is at distance ε from the surface. The blanket thickness is 2ε , for each ε there is an upper surface, u_i, and a bottom surface, b_i (shown in figure 4). An immediate consequence is that these approaches overcoming problems with the scale invariance (expected for fractal dimension in all directions) from the beginning, in the first computation of $N_{(A , \varepsilon)}$. That is, if all gray level direction is translated by adding one box, then the $N_{(A , \varepsilon)}$ will present no variation. Also if the image have its gray scale inverted (black to white or vice-versa) its dimension no change by these methods.

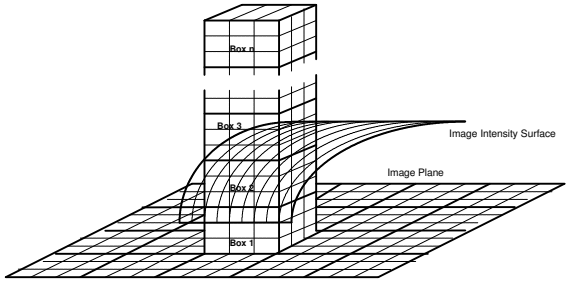

Figure 3 Box-counting on the pixel intensity.

DBC can be easily introduced in equation 2 by computing adequately $N_{(A , \varepsilon)}$. If the minimum gray level of the image in the grid (i,j) fall in box number k, and the maximum gray level of the images on the (i,j)th grid fall in the box number l , then in DBC approach:

$$n(i,j)=l-k+1 \qquad (3)$$

is the blanket thickness on the grid(i,j). Taking contributions from all grids

$$N_{(A , \varepsilon)}=\sum n(i,j) \qquad (4)$$

The FD can be estimate from the least squares linear fit of log x log, after $N_{(A\ ,\ \varepsilon)}$ is counted for different values of boxes dimensions (r and s) .

Although the DBC method gives a very good estimate of FD, some simplifications (in computations) and improvements (in time efficiency) is possible by using the nodifications proposed by Conci and Campos(1996) in the original method. In the so called MDBC - Modified Differential-Box Counting - the image division in box of different length is processed in a new manner from the original DBC method. Consider the image of size MxM pixels, we take M to be a power of 2 and take the range of light intensity to be integers from 0 to 255. All images are enclosed in a big box of size MxMx256. We consider the image divided into box of side length sxsxs' for $s=2,4,8...2^m$ and $s'=2,4....2^{m'}$ for each image subdivision If the minimum gray level of the image in the grid (i , j) fall in box number k, and the maximum gray level of the images (i , j)th grid fall in the box number l , then n is counted as

$$n=int(Gray_max(i,j)/ s'-int(Gray_min(i,j)/ s')+1 \quad (5)$$

where int(..) is the integer part of a division. This change allows the reading of image file only once, in the first image division in boxes of 2x2 pixels. The bitmap of MxM pixels needless be saved, when the image is read we saved only two matrices of M/2xM/2 elements: Gray_max and Gray_min (saving MxM/2). For boxes of 4x4 pixels there will be M/4xM/4 elements in Gray_max and Gray_min, and each new element (i_new,j_new) is obtained from consulting only the four element (i,j); (i+1,j); (i,j+1) and (i+1,j+1) of the Gray_max and Gray_min matrices. In each new iteration the Gray_max and Gray_min matrix elements have half of the length of the last iteration and can be saved in the same area. Then using (2) we estimate FD from averaging of log(N)/log(2n). This method had also be used on color images without simultaneously consideration on all bands (Conci and Proença, 1997) and with high resolution satellite images for texture segmentation (Conci, 1999). This MDBC algorithm and the original BC are used in the next section when the combination of band will be considered. The MDBC method presents also invariance to average gray level, which can be very important in application where the level of illumination can change and modify the texture contrast. For instance, this is the ideal technique for applications on quality control texture applications (Conci and Proença, 1998).

3 Combining bands

Up to now, we have described approaches already used for determination of the FD of binary and monochrome images. These approaches are modeled respectively in the 2-dimensional or 3-dimensional spaces. In synthesis, first they divide the plane ($\Re^2$) in squares or the space ($\Re^3$) in cubes, then they compute the squares or cubes that intercepted the binary or the gray level images respectively. Generalizing, we can suppose that the experimental determination of the FD of multi-channel images (in a multidimensional space $\Re^N$) implies in recursive division of the space in n-dimensional boxes followed by computation of those boxes intercepting the image. For conformity with previous works these n-dimensional boxes are named "n-boxes", n identifies the dimension. Thus, the 1-boxes are a line segment (one-dimensional), the 2-boxes are squares (two-dimensional), the 3-boxes are cubes (three-dimensional), the 4-boxes are hyper-cubes (four-dimensional) and n-boxes refers to n-dimensional spaces.

In b/w images, the 2D space is divided by identical parts of sides L1xL2 (2-boxes). L1 and L2 correspond to the axes of the coordinates 1,2 (figure 1) of the image. In the monochrome images (figure 2), the space 3D is divided by identical parts of sides L1xL2xL3 (3-boxes), where L3 correspond at the intensity level of the image. For color images the space 5D is divided by parts of sides L1xL2xL3xL4xL5 (5-boxes), where L1 and L2 are the pixel coordinates and L3, L4 and L5 the color in the considered color space (usually RGB). In the satellite images, according to the number, c, of considered channels, each axis in the nD space(n=c+2) is divided by the same number of parts resulting the n-boxes, in the n-dimensional space.

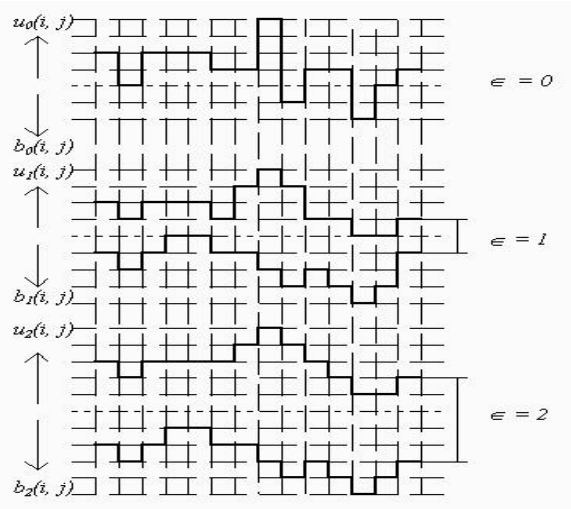

Figure 4 The blanket thickness for different ε

It is difficult, to realize objects with dimension greater than 3D. However, each point in a color image

needs 5 coordinates to be modeled. Pixels on satellite images need more components. To calculate the FD of these images we needed to go besides the third dimension. But how to divide a n-space for computing the n-boxes intersections (being n>3)? How many n-boxes appear in a certain recursive division of the nD space by 1/2? For answer these questions, it is important to observe how known dimensions behave in repeated divisions by half. Note that the number of 1-boxes to 3-boxes in recursive divisions is:

n - dimension	recursive 1/2 division	number of n-boxes
1	2	$4=2^2$
	3	$8=2^3$
	d	$2^d=2^{n.d}$
2	2	$16=2^4$
	3	$64=2^6$
	d	$2^{2.d}=2^{n.d}$
3	2	$64=2^6$
	3	$512=2^9$
	d	$2^{3.d}=2^{n.d}$

That is the number of box depends upon the space n dimension and the number of recursive divisions, d. For 2-boxes it can be determined by $2^{2.d}$. In the same way, for 3-boxes, it is $2^{3.d}$, where d is the number of half divisions. Generalizing, for 4-boxes, 5-boxes or n-boxes, the number of n-boxes is: $2^{d.n}$. For the determination of the n-dimensional FD, the contribution of each channel for the determination of the Nn(n-boxes, d) is made by in accordance with analyzes of the complexity of the blankets the expression:

$n_{channel}(i,j) = int((Max_{channel}(i,j) - Min_{channel}(i,j)) / s') + 1$

Then, results of each half division of the image, N_n(n-boxes,d), can be combined using equations (1) or (2). In the following section the first case are named combination by average and the second least squares fit.

4 Experiments and results

In this section the proposed DBC modifications is used in some experiments. First, the goal is to examine the accuracy of the FD estimation for each channel. Figure 5 shows a classical example of fractal and its FD reached by the implementation. Several others well known fractals can have their fractal dimension computed when considered by this approach as Black and White images.

For a second group of experiments, using only one band, the Brodatz's textures on figure 6 are used. Table 1 compares the results of present work with others, in which intensity level images can be analyzed. In these results, the implementation uses 3-boxes of sides 2,4,8,16, and 32 on the procedure that combines recursive division by the average , column 9. For the line fitting procedure (column 10) all recursive division are used (that is, for these texture samples of 256x256x256, each image division goes from 2097152 boxes with 2x2x2 to 8 boxes of 128x128x128).

On the screen zoom showed on figure 7, the two implemented combination of all 7 channels (by averaging or line fitting the 9-boxes at all resolution) can be seem. For these results, in multiband combination, we used the images from LANSAT 7 on figure 8 to 10. In these figures the color images on the left is the band combination in analyze displayed as R,G or B. It is possible to display whatever band combination, wanted by the user. On figure 8 the usual combination of the visible channels creates a natural-looking image. On the table, presented on the screen, in fig. 8 it is possible to see the FD of each channel and the results of these 3 channels together in the 5D row. On figure 9, the combination of the near-infrared Band 4, with mid-infrared Band 5 and the thermal infrared Band 6 adds subtle details, not readily apparent in the visible band. Although, all images represent the same place, each band combination to RGB produce a diferrent image. Also, on the table of figure 9, it is possible to see the obtained FD by each channel, and the results of these 3 channels together on the 5D row. Figure 10 shows the implementation results of mid infrared band 7.

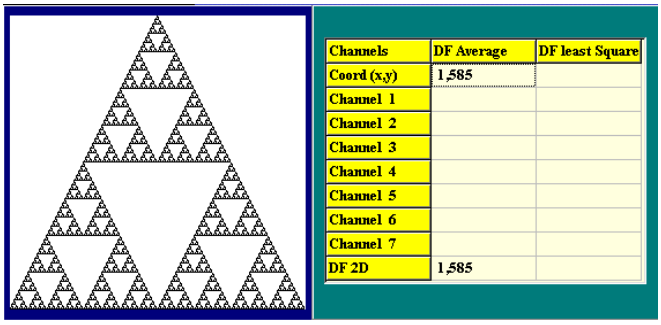

Figure 5 DF Sierpinski gasket (ln3/ln2= 1.58496....)

5 Conclusions

Multi-band combination in image fractal analysis has been introduced in this paper,. Well know fractals and several images of "Brodatz textures", with their fractal dimension computed by various methods, were used to illustrate the efficiency of this approach to find FD for each band or for Black and White images.

Of course, figures of classical Fractal Geometry are calculate with advantage using theoretical definitions of dimension. Here, they have been used only to show the correction of the implementation. This situation is changed when experimental techniques are compared. Roughly speaking, table 1 says that each implementation presents special properties and consequences. We might hope to

explain something by not restricting the attention to results. Pentland (1984) suggested a method of estimating FD by using Fourier power spectrum of image intensity surface, such method gives satisfactory results but, since this Fourier transformation computation is included, it is slower than the others. Peleg et al (1984) extended fractal idea to image, they drove image vision as a terrain surface whose height is proportional to the image gray value. The *reticular cell counting* estimator has been proposed by Gangepain and Roques-Carmes (1986). But this estimator can only be used when the range of the actual FD of an image is from 2.0 to 2.5. Parker (1997) uses Hurst coefficient as an approximation of equation (1) for gray level images, but this coefficients turn possible results out of the theoretical range expected for images, that is the interval [2 ,3]. Voss (1986) refers to *box counting* as the process of estimating the probability that *m* points lie in the box. Keller et al. (1989) proposed a modification of the method due to Voss, which presents satisfactory results up to FD=2.75. Sarkar and Chaudhuri (1994) described an efficient box-counting approach, named *Differential Box-Counting* (DBC), that uses differences on computing N_r , and gives satisfactory results in all range of FD. In Conci and Campos(1996) fast computation and identification of image variations were the main goal, so the results considered only the average and the minimum number of image box division. In the opposite end is the work of Coelho and Conci (2001) that looks for correction of results on comparison with an experimental Hausdorff Dimension approach. This work uses cubes of all the possible sizes (considering sides of 2, 3, 5, 6, 9, 10, 12, 15, 18, 20, 30, 36 and 45 pixels) with or without superposition and several curve fittings. It also considers the possibility of using thermal channels for image threshold before calculation of FD.

The main aspect of the present work are the possibilities opened by using all the Landsat bands and fractal dimension for texture classification. The examples show the possibilities of the proposed technique, that is the only that uses band's reciprocal action. Although others works have used satellite images ans fractal geometry only one channel have been used on anallysis (Carvalho and SilvaDias, 1998). The modification used in Buchnicek at al. (2000) consists of counting separately squares (2d elements, no 3d boxes), which are completely black and separately squares, which cover border of black object, e.g. those squares which contain at least part of the tested black object and obtain three fractal dimensions which characterize properties of black plane, black-white border of black object. Altought image information can be handled in four color spaces - intensity (shades of gray), HSB/HSV (hue, saturation, brightness/value), HLS (hue, lightness, saturation) and RGB (red, green and blue channel) in HARFA, (Buchnicek at al., 2000: http://www.fch.vutbr.cz/lectures/imagesci/harfa.htm) for FD determination they use only images in B&W. HarFA examines fractal structures which come into existence during process they called "masking". Masking transforms colored image object into black&white one. There are many criteria which can be changed to derive many different fractal structures from one image (e.g. it can alter minimal value of hue to be masked as black one, or it can determine that black will be all pixels which fulfil conditions of their RGB channels). So they can get various fractal dimensions for one image. If the point is to characterize image by its fractal dimension, how know which of them is appropriate. So it is impossible compare our results on bands with HarFA results because all 3D information on the image will be lost.

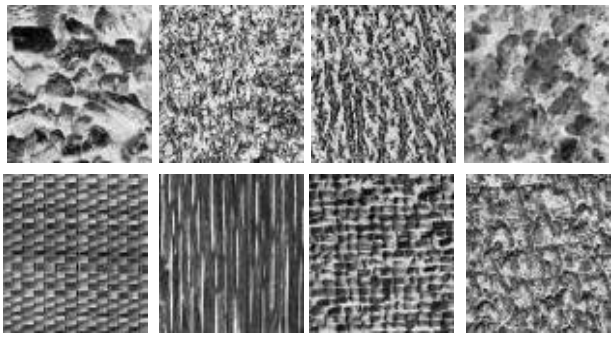

Figure 6 Bordatz's Textures [16]: D05,D09, D24, D28, D55, D68, D84 and D92, used on table 1 experiments.

Channels	DF Average	DF least Square
Coord (x,y)		
Channel 1	2,856	2,537
Channel 2	2,871	2,601
Channel 3	2,881	2,634
Channel 4	2,885	2,620
Channel 5	2,886	2,626
Channel 6	2,845	2,524
Channel 7	2,872	2,572
DF 9D	8,236	6,546

Figure 7 Zoom on the result of combining all 7 bands counting the 9-boxes and combining all bands for both procedures

6 Acknowledgment

This work was supported by the project CNPq/PROTEM-CC(Quali-In).

References

[1]K. Falconer, K., *Techniques in Fractal Geometry*, John Wiley & Sons Ltd., England (1997).

[2]A. Conci and C.B. Proenca, "A Box-Counting Approach to Color Image Segmentation", *Proceedings of IEEE International Conference on Image Processing* ICIP'97,Santa Barbara, USA, 1(1997) 1265--1268

[3]A. Conci and C.B. Proenca, "A fractal image analysis system for fabric inspection based on a box-counting method, *Computer Networks and ISDN Systems*, Elsevier Science, 30, Issue 20-21,(1998), 1887--1895.

[4]A. Conci, "Texture Classification of Lansat Images Using Fractal Dimension and Bands", CD-ROM do GisBrasil (1999).

[5]A. Conci and L. H. Monteiro, "Multifractal Characterization of Texture Based Segmentation", Proceedings of IEEE International Conference on Image Processing, Vancouver, Canada, 1 (2000), 792--795.

[6]F. F. S. Coelho and A. Conci, "An Efficient Approach to Compute the Hausdorff Dimension of Images", to appear at *Proc. of IEEE - EURASIP Workshop on Nonlinear Signal and Image Processing*, Baltimore, Maryland USA. (2001)

[7]Q. Jiang and T. Keaton, "Automatic Extraction of Urban Regions from multispectral spot satellite imagery", *Proceedings of IEEE International Conference on Image Processing ICIP*, Vancouver, Canada, 2 (2000), 728-731.

[8]V. Lakshmanan, V. DeBrunner and R. Rabin, "Texture-Based Segmentation of Satellite Weather Imagery", Proc. IEEE International Conference on Image Processing, Vancouver, Canada, 2000, vol. 2, 732--735.

[9]AJ. Gangepain and C. Roques-Carmes,1986: "Fractal approach to two dimensional and three dimensional surface roughness", *Wear,* Vol. 109, 119--126.

[10]S. Peleg, J. Naor, R. Hartley and D. Avnir, 1984: "Multiple resolution texture analysis and classification", *IEEE Trans. Pattern Anal. Mach Intell.,* Vol. 6, 518--523.

[11]N. Sarkar and B. B. Chaudhuri, "An efficient differential box-counting approach to compute fractal Dimension of Image", *IEEE Trans. Syst. Man and Cyber.,* 24, No.1, (1994), 115--120.

[12]J. R. Parker, *Algorithms for Image Processing and Computer Vision,* John Wiley & Sons, Toronto (1997)

[13]`M. Buchnicek, M. Nezadal and O. Zmeskal, "Numerical Calculation of Fractal Dimension", *Nostradamus 2000 - Prediction Conference*, Zlin, Czech Republic, (2000), http://www.fch.vutbr.cz/lectures/imagesci/harfa.htm.

[14] J. Keller, R. Crownover and S. Chen, "Texture description and segmentation through fractal geometry", *Computer Vision Graphics Image Proc.*, (1989) 150--160.

[15]A. P. Pentland, "Fractal based description of natural scenes", *IEEE Trans. Pattern Analysis Machine Intell*., 6, (1984) 661--674.

[16]P. Brodatz, *Textures: A photographic Album for Artists and Designers*, New York, Dover, (1966) from:. http://www.ux.his.no/~tranden/brodatz.html (2001).

[17]A. Conci and C.F.J. Campos, "An Efficient Box-Counting Fractal Dimension Approach for Experimental Image Variation Characterization", Proc. IWISP, Manchester, (1996) 665--668.

[18]R. Voss, "Random fractals: Characterization and measurement", in Scaling Phenomena in Disordered Systems, R. Pynn and A. Skjeltorp Eds., Plenum (1986).

[19]L.M.V. Carvalho abd M.A.F.Silva Dias, "An aplication of Fractal Box-Dimension to the Recognition of Mesoscale Cloud Pattern in iNfrared Satellite Images", Journal of Applied Meteorology (1998), 1265--1288.

Image	Conci[17]	Pentland[15]	Coelho[6]	Keller[14]	Sarkar[11]	Peleg [10]	Gang.[9]	Average	Line Fit
D05	2.45	2.38	2.67	2.57	2.45	2.52	2.38	2,77	2,49
D09	2.58	2.49	2.75	2.65	2.59	2.65	2.43	2,70	2,46
D24	2.44	2.46	2.78	2.57	2.45	2.59	2.39	2,76	2,51
D28	2.55	2.48	2.61	2.62	2.55	2.61	2.41	2,76	2,51
D55	2.48	2.37	2.70	2.59	2.48	2.60	2.39	2,69	2,46
D68	2.53	2.44	2.57	2.60	2.52	2.63	2.40	2,74	2,47
D84	2.61	2.47	2.75	2.65	2.60	2.68	2.43	2,75	2,47
D92	2.50	2.38	2.69	2.59	2.50	2.59	2.41	2,81	2,58

Table 1 Comparison of FD among various works (image numbers correspond to Brodatz's book)

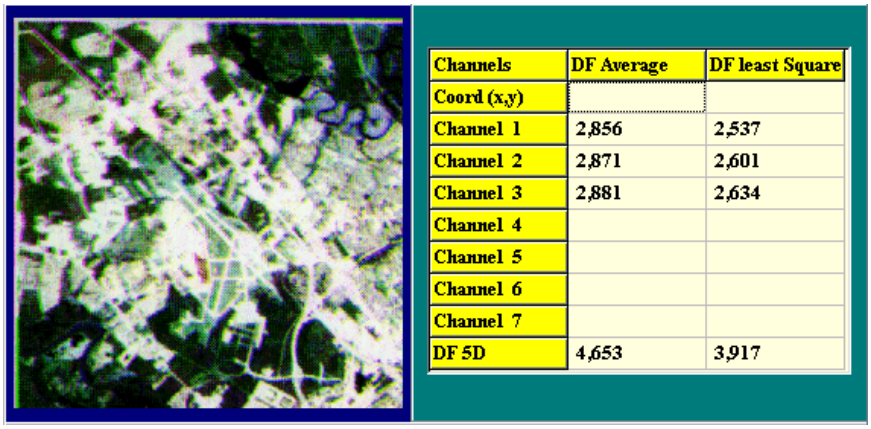

Channels	DF Average	DF least Square
Coord (x,y)		
Channel 1	2,856	2,537
Channel 2	2,871	2,601
Channel 3	2,881	2,634
Channel 4		
Channel 5		
Channel 6		
Channel 7		
DF 5D	4,653	3,917

Figure 8 Bands 1,2,3 as RGB images on the left. In the table, FD of each band and their combination by counting 5-box for both implemented procedures

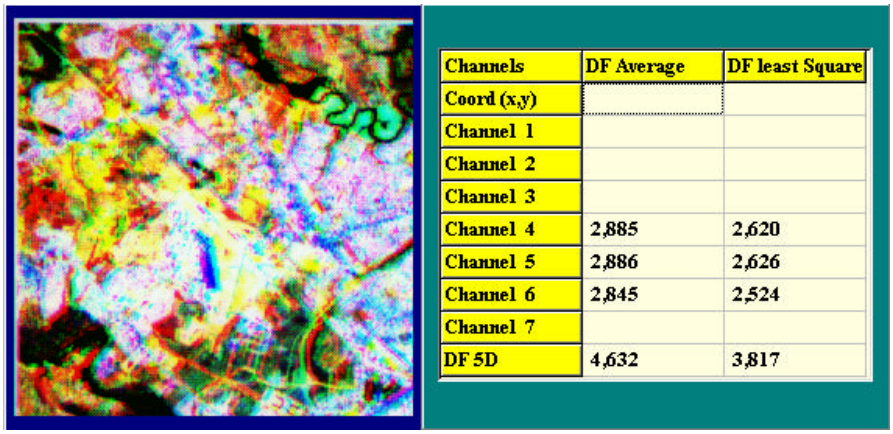

Channels	DF Average	DF least Square
Coord (x,y)		
Channel 1		
Channel 2		
Channel 3		
Channel 4	2,885	2,620
Channel 5	2,886	2,626
Channel 6	2,845	2,524
Channel 7		
DF 5D	4,632	3,817

Figure 9 Bands 4,5,6 as RGB images on the left. In the table, FD of each band and their combination by counting 5-box for both implemented procedures

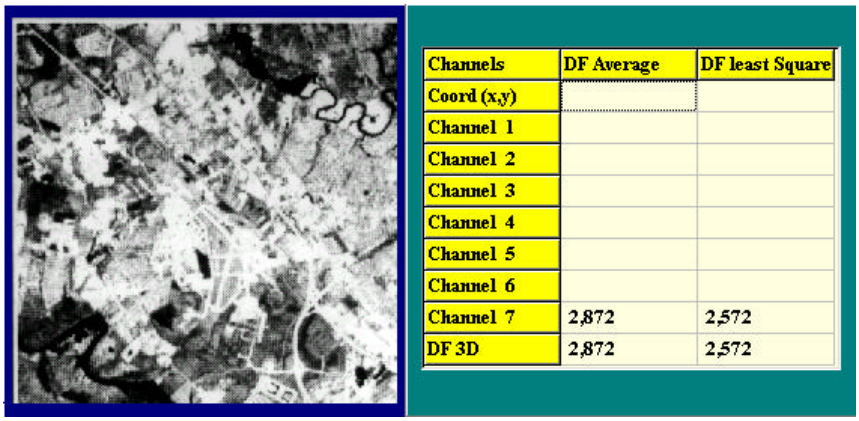

Channels	DF Average	DF least Square
Coord (x,y)		
Channel 1		
Channel 2		
Channel 3		
Channel 4		
Channel 5		
Channel 6		
Channel 7	2,872	2,572
DF 3D	2,872	2,572

Figure 10 Band 7 as gray level image on the left. In the table, FD for this band counting 3-box for both implemented procedures.